Nanoparticles in MOFs

DOI: 10.1002/anie.201202549

Nanoparticle Core/Shell Architectures within MOF Crystals Synthesized by Reaction Diffusion**

*Yanhu Wei, Shuangbing Han, David A. Walker, Patrick E. Fuller, and Bartosz A. Grzybowski**

Metal–organic frameworks (MOFs) have attracted considerable attention on account of their applications in molecular separations,[1] gas storage,[2] catalysis,[3] and chemical sensing.[4] Recently, there has been a growing interest in using these highly ordered microporous architectures as host matrices or templates with incorporated metal or metal oxide nanoclusters or nanoparticles (NPs).[5] Such hybrid NP-MOF structures are promising materials for gas storage and catalysis.[6] The strategies available for the incorporation of metal or metal oxide NPs into MOFs include solvent-free gas-phase loading,[7] solution impregnation,[6c,8] incipient wetness impregnation,[5a,9] solid grinding,[10] and microwave irradiation.[11] Most of these techniques, however, involve relatively cumbersome processes such as pretreating the MOF (e.g., by solvent exchange or MOF activation)[7,8c] or particle loading (by introduction of reducing agents,[11,12] heating,[6a,8c] irradiation,[12,13] etc.), and none allows any spatial control over the NP loading within the MOF crystals. Here, we describe a procedure in which reaction-diffusion[14] processes inside the MOF crystals mediate the deposition of NPs either in a uniform or in a location-specific fashion, with the latter leading to the formation of core/shell architectures (which are of interest in the context of multistep catalysis).[14d,15] In our method, cyclodextrin-based MOF (CD-MOF) crystals[4b,16] are immersed in a metal (here, Ag or Au) salt solution, and the OH^- counterions—which are homogenously distributed in the CD-MOF at concentrations of about 1.33 M—reduce this salt to the respective metal NPs. By coupling the diffusion of salt precursors with their reduction inside the CD-MOFs it is possible to deposit the NPs only at the core of the MOF crystal and such that the thickness of the NP-free shell depends on the concentration of the $HAuCl_4$ used. Subsequent deposition of another type of NPs gives rise to core/shell architectures. NPs of all types can be readily liberated by dissolving the CD-MOFs in water—for the core/shell NP/CD-MOFs, the release of the two different types of NPs is then sequential.

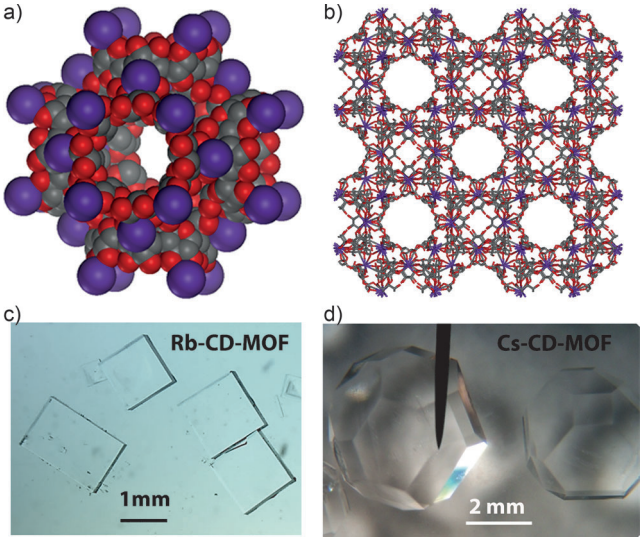

Figure 1. a) A unit cell of Rb- or Cs-CD-MOF crystals synthesized from γ-CD and RbOH or CsOH, respectively (red: oxygen; gray: carbon; purple: Rb or Cs). b) The 1D channels in Rb- or Cs-CD-MOF crystals. c) and d) The optical images of the millimeter-sized Rb-CD-MOF and Cs-CD-MOF crystals, respectively.

Two types of millimeter-sized CD-MOFs were used. The first type was synthesized from γ-cyclodextrin (γ-CD) and RbOH following the reported procedures[4b,16] (see Experimental Section for details). As illustrated in Figure 1 a–c, these Rb-CD-MOF single crystals[4b] (for powder X-ray diffraction (PXRD) spectra, see Section 1 in the Supporting Information) were rectangular prisms up to about $2\times2\times1$ mm in size with nanosized cavities (ca. 1.7 nm across) and 1D channels connecting them (channel cross-section: ca. 8×8 Å^2). The second type of MOF was also made from γ-CD, but CsOH was used as the alkali metal source. These Cs-CD-MOF crystals[16] also comprised cavities of approximately 1.7 nm in diameter connected by channels with cross-sections of about 8×8 Å^2 (Figure 1 a,b). Following the procedure described in the Experimental Section, Cs-CD-MOF single crystals were grown that had an overall truncated-octahedron shape and the diameters of these crystals were up to 5 mm (Figure 1 d, see also the PXRD spectra in Section 2 of the Supporting Information).

In the context of the present work, the key feature of the CD-MOFs is that they contain hydroxide counterions (one per metal center) which can work either alone or cooperatively with the cyclodextin units to reduce metal salt

[*] Dr. Y. Wei,[+] Dr. S. Han,[+] D. A. Walker, P. E. Fuller, Prof. Dr. B. A. Grzybowski
Department of Chemical and Biological Engineering Department of Chemistry, Northwestern University
2145 Sheridan Rd., Evanston, IL 60208 (USA)
E-mail: grzybor@northwestern.edu
Homepage: http://dysa.northwestern.edu

[+] These authors contributed equally to this work.

[**] This work was supported by the Non-equilibrium Energy Research Center, which is an Energy Frontier Research Center funded by the U.S. Department of Energy, Office of Science, Office of Basic Energy Sciences under Award Number DE-SC0000989.

Supporting information for this article is available on the WWW under http://dx.doi.org/10.1002/anie.201202549.

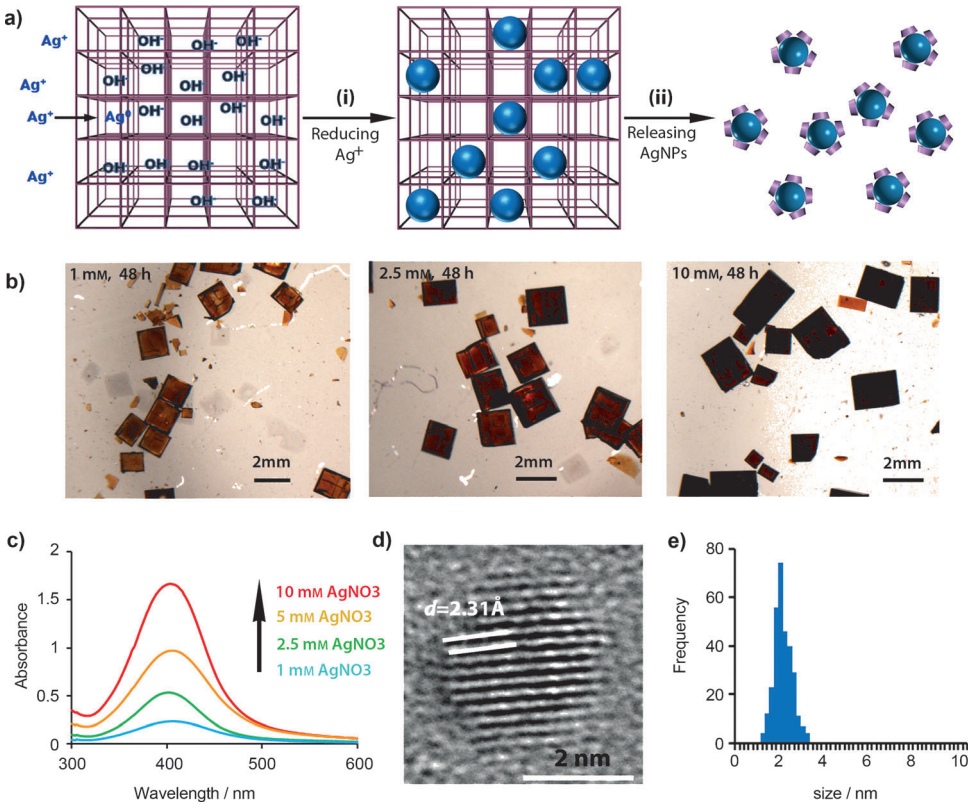

Figure 2. a) Scheme illustrating the diffusion and reduction of Ag^+ ions within CD-MOFs, as well as the release of the Ag NPs formed when the MOF crystal is dissolved in water. The liberated NPs are stabilized in solution by cyclodextrin molecules.[18] b) Color changes of Rb-CD-MOF crystals upon immersion in acetonitrile solutions of different $AgNO_3$ concentrations. c) UV/Vis spectra of AgNPs formed in Rb-CD-MOFs by soaking these crystals for 48 h in 1–10 mM solutions of $AgNO_3$ in acetonitrile. d) A typical HRTEM image of an Ag NP synthesized in a Rb-CD-MOF crystal. e) A histogram of Ag NP sizes (statistics based on 360 particles from three independent experiments).

precursors to their respective NPs (see Section 6 in the Supporting Information). This is illustrated schematically in Figure 2a, while Figure 2b shows the optical images of Rb-CD-MOF crystals soaked in 1.0, 2.5, and 10 mM solutions of $AgNO_3$ in acetonitrile. This procedure deposits Ag NPs throughout the entire MOF crystal. The amount of deposited Ag NPs increases on either increasing the time of soaking or with increasing $AgNO_3$ concentration, as reflected by the color change of the crystals (from yellow to brown-orange, to dark brown-orange; Figure 2b). Analysis of the MOFs by inductively coupled plasma atomic emission spectroscopy (ICP-AES) demonstrates that when the concentrations reach steady-state values at 48 h of soaking, the content of silver is about 1.2% (w/w) for $[AgNO_3] = 1$ mM and 4% for $[AgNO_3] = 10$ mM (see Section 3 in the Supporting Information).

To ascertain that the deposition of silver corresponded to the formation of Ag NPs, the MOF crystals were dissolved in water, to give orange-yellow solutions, whose UV/Vis spectra featured a characteristic Ag surface plasmon resonance (SPR) band at about 410 nm (Figure 2c). High-resolution transition electron microscopy (HRTEM) imaging (Figure 2d) confirmed the presence of approximately 2.0 nm diameter Ag NPs, with the lattice spacing of $d = 2.31$ Å consistent with the reported spacing of Ag{111} facets.[17] The histogram of particle sizes in Figure 2e shows the range of Ag NP sizes to be (2 ± 0.4) nm (also see the large-domain TEM image in Section 4 and phase-transfer experiments in Section 5 of the Supporting Information).

While nanoparticles are also produced inside CD-MOFs by using a gold salt precursor ($HAuCl_4$), this process is markedly slower than the deposition of Ag NPs (possibly because multiple electrons are required for the reduction of Au^{III}; see Section 6 in the Supporting Information) and, by virtue of the reaction and diffusion occurring on similar time scales, leads to the formation of an Au NP "core" inside the MOF crystal (Figure 3a–d). Specifically, when the CD-MOF crystals were immersed in 0.5–10 mM acetonitrile solutions of $HAuCl_4$, the formation of Au NPs was evidenced by the color of the MOFs changing to red. After dissolution of the MOF, the NPs were characterized by HRTEM and TEM (Figure 3f, and see Section 7 in the Supporting Information) as being about 3–4 nm in diameter (with the lattice spacing, $d = 2.41$ Å, consistent with the reported value for Au{111} facets[19]), and their solutions exhibited a strong Au SPR band at 520 nm (the UV/Vis spectrum is shown in Section 7 of the Supporting Information). However, the deposition of the NPs was not uniform throughout the MOF crystal—instead, the NPs were found predominantly in the core of the crystal, surrounded by a clear, NP-free peripheral region (ICP elemental analysis indicated that 95% of all the NPs within the crystal are within the core).

We observe that the thickness of the NP-free, "shell" region (d_{free}) increases as the concentration of the $HAuCl_4$ salt increases. This trend reflects a process in which the gold salt migrating into the crystal reacts with the hydroxide ions, nucleates the growth of Au NPs, and, in doing so, modifies local concentration gradients along which Au^{III} and OH^- species diffuse. The coupling between reaction and diffusion can be quantified in the form of a reaction-diffusion model (described in detail in Section 8 of the Supporting Information). It is noteworthy that this model reproduces faithfully the nonlinear dependence between d_{free} and parameter γ, which is the ratio of the concentrations of the gold salt in solution and the hydroxide ions in the MOF (Figure 3e).

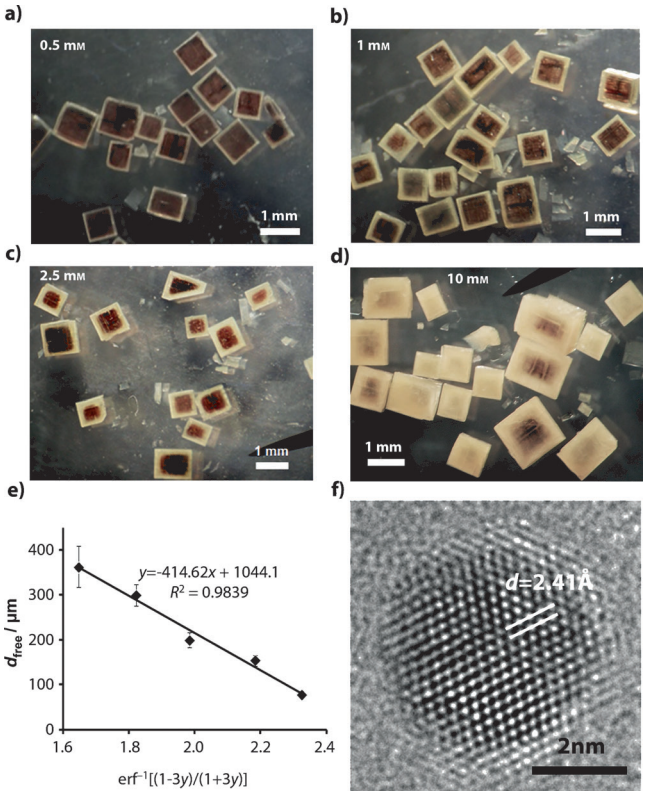

Figure 3. Optical images of Rb-CD-MOF crystals with differently sized Au NP cores formed using solutions of $HAuCl_4$ in acetonitrile at concentrations of a) 0.5 mM, b) 1 mM, c) 2.5 mM, and d) 10 mM. e) The experimentally observed thickness d_{free} of the NP-free clear shell (markers) agrees with the trend $d_{free} \approx \mathrm{erf}^{-1}[(1-3\gamma)/(1+3\gamma)]$, predicted by reaction-diffusion modeling (solid line); erf stands for error function, and parameter γ is the ratio of the $HAuCl_4$ solution concentration and OH^- concentration in the MOF. Error bars correspond to standard deviations based on the analysis of 20 crystals from 3 independent experiments. f) A high-resolution TEM image of a typical Au NP synthesized within the Rb-CD-MOF and released by dissolving the MOF crystal in water. The white lines illustrate the $d = 2.41$ Å spacing between the Au{111} planes.

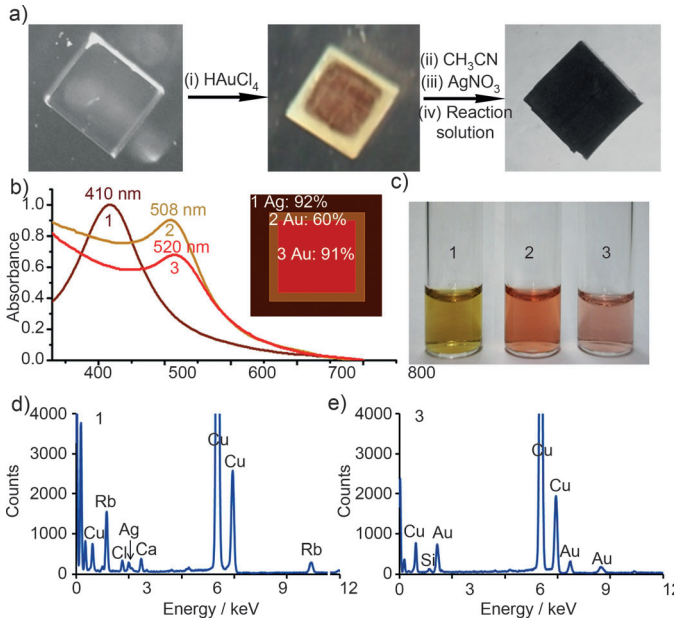

Figure 4. a) Optical images of Rb-CD-MOF first loaded with Au NPs in the core region, and then with Ag NPs in the shell region. b) The UV/Vis spectra demonstrate that gradual dissolution of the core/shell CD-MOF first liberates predominantly the Ag NPs from the shell region (SPR band at ca. 410 nm), and then the Au NPs from the core region (SPR band at ca. 520 nm). The inset delineates schematically the regions corresponding to the UV/Vis spectra and also gives the approximate elemental composition of Ag and Au determined by the ICP-EAS of the dissolved NP/MOF solutions (outermost region 1: thickness ca. 150 µm, composition > 90% Ag and < 10% Au; "intermediate" region 2: thickness ca. 50 µm, composition ca. 40% Ag and ca. 60% Au; innermost region 3: thickness ca. 1000 µm, composition < 10% Ag and > 90% Au). c) Optical images of the solutions corresponding to the regions 1, 2, and 3 indicated in the inset of (b). The EDX spectra acquired from corresponding solutions: d) 1 and e) 3.

The combination of the deposition modes of Ag and Au allows for the synthesis of core/shell CD-MOFs. The sequence of steps is outlined in Figure 4a—first, a core of Au NPs is formed by immersion of crystals in $HAuCl_4$. This is followed by washing them with acetonitrile and immersion in $AgNO_3$ to deposit Ag NPs in the shell region (see Experimental Section for details). The compositions of these regions were examined in three ways: 1) by gradually dissolving the MOFs, collecting the particles thus released, and recording the UV/Vis spectra of the NP solutions (Figure 4b); 2) by ICP-AES analysis of these solutions (see inset to Figure 4b); and 3) by recording the energy-dispersive X-ray (EDX) spectra of the corresponding solutions 1 and 3 (Figure 4d,e). All of these studies confirmed a core/shell architecture in which the outermost/shell region had an elemental content of Ag > 90% (and < 10% Au), and with the innermost core region comprising over 90% Au. The relative dimensions of the Ag-rich and the Au-rich regions could be adjusted by changing the core size, as described above and illustrated in Figure 3.

We make two further comments regarding these core/shell structures. First, the NP deposition procedures described above worked best in acetonitrile. Although the reduction of metal salts proceeds much faster in methanol, this solvent could not be used as it caused degradation of the MOF scaffolds (see Section 9 and Figure S15 in the Supporting Information)—as a result, the NPs that were formed were ill-shaped and within minutes they also coalesced into larger aggregates. Second, once the NPs were made within the MOF crystals, it was possible to perform galvanic exchange reactions by immersing these crystals into a solution of a metal salt of cations having a higher redox potential. One example is illustrated in Figure 5, where Cs-CD-MOF crystals were first uniformly loaded with Ag NPs, which were then partly (after ca. 3 h; Figure 5b,c) exchanged for Au NPs. An interesting feature of this process is that because the exchange occurs relatively slowly, the NP composition within a MOF can form a smooth gradient with the shell regions richer in Au NPs and the core regions richer in Ag NPs. Of course, with longer reaction times (ca. 9–10 h, Figure 5d,e), almost all of the Ag NPs within the MOF are exchanged for Au NPs. Finally, our preliminary results indicate that exchange of Ag NPs by catalytically active Pd NPs (using $Pd(NO_3)_2$ as a salt

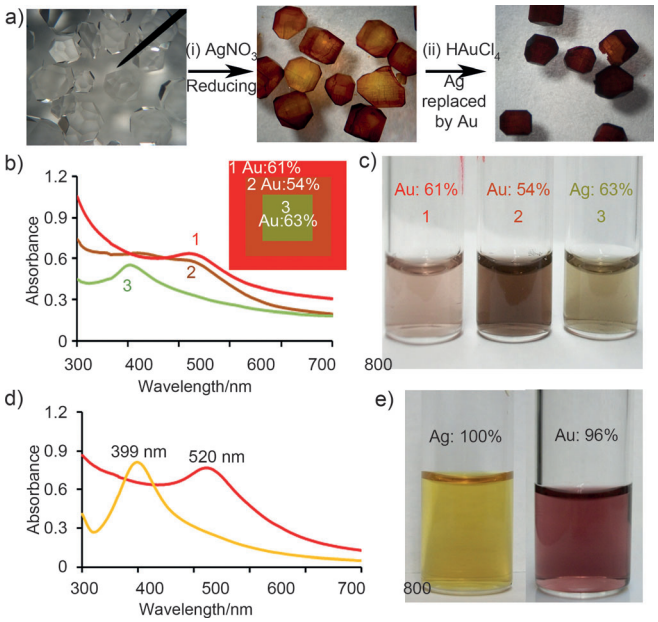

Figure 5. a) Optical images of Cs-CD-MOF crystals first loaded with Ag NPs, and then partly converted into Au NPs in the shell region by galvanic exchange reactions. b) The UV/Vis spectra demonstrate the Au NP rich shell region (SPR band at ca. 520 nm) and the Ag NP rich core (SPR band at ca. 410 nm) after 3 h of reaction time. The inset delineates schematically the regions corresponding to the UV/Vis spectra and also gives the approximate elemental composition of Ag and Au determined by the ICP-EAS of the dissolved NP/MOF solutions (outermost region 1: thickness ca. 500 μm, composition ca. 39% Ag and ca. 61% Au; "intermediate" region 2: thickness ca. 300 μm, composition ca. 46% Ag and ca. 54% Au; innermost region 3: thickness ca. 1000 μm, composition ca. 63% Ag and ca. 37% Au). c) Optical images of the solutions corresponding to the regions 1, 2, and 3 indicated in the inset of (b). d) The UV/Vis spectra of an aqueous solution of freshly synthesized Ag NP/Cs-CD-MOFs (orange curve) and Ag NP/Cs-CD-MOFs after 9 h of galvanic exchange reaction (red curve) demonstrate almost complete replacement of Ag NPs by Au NPs. e) Optical images of the corresponding Ag NP and Au NP solutions. ICP analyses show that 96% of Ag was replaced by Au after 9 h of galvanic reaction.

precursor) is also feasible, although the kinetics of this process is slower than that of Ag-to-Au exchange. After 20 h of galvanic reaction, about 86% of the Ag NPs in the MOFs were replaced by Pd NPs (see Section 10 and Figure S16 in the Supporting Information).

In summary, we combined the reductive properties of CD-MOF interiors with the diffusive transport of metal salts to deposit metal NPs either uniformly throughout the MOF or in a core/shell manner. The core/shell MOF architectures are interesting for two main reasons. First, when being dissolved, they can mediate the controlled delivery of NPs, which could be potentially useful because of the antibacterial Ag and Au NPs and the nontoxic—in fact, edible[16]—CD-MOFs. Second, when extended to other types of catalytically active NPs (e.g., Pd, Pt), the core/shell MOFs can direct sequential reactions on the substrates diffusing from the outside toward the center of the MOF crystals. We have recently validated this concept with core/shell arrangements of NPs suspended in solvent-permeable polymers.[14d] MOFs can extend the capabilities of such systems by virtue of their nanoscopic channels providing substrate specificity (i.e., permitting only certain substrates to diffuse into the crystal, see Ref [1a, 4b]).

Experimental Section

1. Preparation of Rb-CD-MOF single crystals: In a typical procedure, γ-CD (5.2 g, 4 mmol) and RbOH (3.28 g, 32 mmol) were dissolved in deionized H_2O (80 mL). After filtering the mixture through a syringe filter (0.45 μm PTFE membrane), the clear solution was divided evenly into 16 prewashed vials (5 mL per vial). MeOH (ca. 50 mL) was allowed to vapor-diffuse slowly into the vials over a period of 3 to 7 days. Millimeter-sized, colorless cubic Rb-CD-MOF crystals (up to ca. $2 \times 2 \times 1$ mm) were isolated and washed with MeOH and CH_3CN prior to use.

2. Preparation of Cs-CD-MOF single crystals: γ-CD (1.3 g, 1 mmol) and CsOH (1.34 g, 8 mmol) were dissolved in deionized H_2O (20 mL). After filtering the mixture through a syringe filter (0.45 μm PTFE membrane), the clear solution was divided evenly into five prewashed vials (4 mL per vial). MeOH or EtOH (ca. 50 mL) with a small amount of water (ca. 0.5 mL) was allowed to vapor-diffuse slowly (*important*!) into the vials over a period of 5 to 10 days. Millimeter-sized, truncated-octahedron Cs-CD-MOF crystals (up to ca. 5 mm in diameter) were isolated and washed with CH_3CN and stored in CH_3CN until used.

3. Synthesis of NP-loaded MOFs: In a typical procedure, 20 pieces of millimeter-sized CD-MOF crystals were immersed in acetonitrile solution of $AgNO_3$ (2.5 mM) or $HAuCl_4$ (1 mM) for 24 h for Ag and 60 h for Au. The as-prepared Ag or Au NP/CD-MOF crystals were removed from the reaction solution and washed with fresh acetonitrile several times over 24 h to completely remove the remaining salts. The crystals were dissolved in deionized water to obtain water-soluble Ag/Au NPs.

4. Synthesis of Au/Ag core/shell MOFs: Typically, ten Rb-CD-MOF or Cs-CD-MOF crystals were immersed in a solution of $HAuCl_4$ in acetonitrile (2 mM) for 48–60 h to form an Au NP core inside the CD-MOFs. The freshly prepared Au NP/CD-MOF crystals were removed from the reaction solution, washed with fresh acetonitrile to completely remove the remaining $HAuCl_4$ salts, and then immersed in $AgNO_3$ (5 mM) solution for 1 h, followed by 30 min immersion in the reaction solution originally used to synthesize the CD-MOFs (this allowed more OH^- to diffuse into the MOF to help reduce $AgNO_3$). The prepared Au/Ag core/shell/CD-MOF crystals were gradually dissolved in deionized water and the NP fractions were collected for UV/Vis spectroscopic, ICP, and EDX analyses.

5. Synthesis of gradient Ag/Au core/shell MOFs by galvanic exchange: Typically, about 20 pieces of millimeter-sized Rb-CD-MOF or Cs-CD-MOF crystals were immersed in a solution of $AgNO_3$ in acetonitrile (5 mM) for 24 h to form Ag NP/CD-MOFs. The freshly prepared Ag NP/CD-MOF crystals were removed from the reaction solution, washed with acetonitrile, and then added to a flask charged with a solution of $HAuCl_4$ (0.5–1 mM) in acetonitrile (6 mL) followed by heating at reflux under Ar for 3 h. During reflux, Ag NPs were gradually replaced by Au NPs by galvanic reaction. The prepared Ag/Au core/shell/CD-MOFs were washed with fresh acetonitrile several times to completely remove the remaining $HAuCl_4$ salts. The compositions of different regions within the MOF were examined by gradually dissolving the crystals in deionized water and analyzing the NP fractions by UV/Vis spectroscopy and ICP analysis.

Received: April 2, 2012
Published online: June 29, 2012

Keywords: core–shell structures · metal–organic frameworks · microporous materials · nanoparticles · reaction diffusion

[1] a) S. Han, Y. Wei, C. Valente, I. Lagzi, J. J. Gassensmith, A. Coskun, J. F. Stoddart, B. A. Grzybowski, *J. Am. Chem. Soc.* **2010**, *132*, 16358 – 16361; b) J. R. Li, R. J. Kuppler, H. Zhou, *Chem. Soc. Rev.* **2009**, *38*, 1477 – 1504; c) Z. Y. Gu, L. P. Yuan, *Angew. Chem.* **2010**, *122*, 1519 – 1522; *Angew. Chem. Int. Ed.* **2010**, *49*, 1477 – 1480.

[2] a) W. Zhou, H. Wu, T. Yildirim, *J. Am. Chem. Soc.* **2008**, *130*, 15268 – 15269; b) L. J. Murray, M. Dincă, J. R. Long, *Chem. Soc. Rev.* **2009**, *38*, 1294 – 1314.

[3] a) L. Ma, J. M. Falkowski, C. Abney, W. Lin, *Nat. Chem.* **2010**, *2*, 838 – 846; b) D. Farrusseng, S. Aguado, C. Pinel, *Angew. Chem.* **2009**, *121*, 7638 – 7649; *Angew. Chem. Int. Ed.* **2009**, *48*, 7502 – 7513; c) K. P. Lillerud, U. Olsbye, M. Tilset, *Top. Catal.* **2010**, *53*, 859 – 868.

[4] a) G. Lu, J. T. Hupp, *J. Am. Chem. Soc.* **2010**, *132*, 7832 – 7833; b) S. Han, Y. Wei, C. Valente, R. S. Forgan, J. J. Gassensmith, R. A. Smaldone, H. Nakanishi, A. Coskun, J. F. Stoddart, B. A. Grzybowski, *Angew. Chem.* **2011**, *123*, 290 – 293; *Angew. Chem. Int. Ed.* **2011**, *50*, 276 – 279; c) N. B. Shustova, B. D. McCarthy, M. Dincă, *J. Am. Chem. Soc.* **2011**, *133*, 20126 – 20129.

[5] a) M. Meilikhov, K. Yusenko, D. Esken, S. Turner, G. V. Tendeloo, R. A. Fischer, *Eur. J. Inorg. Chem.* **2010**, 3701 – 3714; b) F. Schröder, R. A. Fischer, *Top. Curr. Chem.* **2010**, *293*, 77 – 113.

[6] a) S. Proch, J. Herrmannsdörfer, R. Kempe, C. Kern, A. Jess, L. Seyfarth, J. Senker, *Chem. Eur. J.* **2008**, *14*, 8204 – 8212; b) H.-L. Jiang, B. Liu, T. Akita, M. Haruta, H. Sakurai, Q. Xu, *J. Am. Chem. Soc.* **2009**, *131*, 11302 – 11303; c) Y. Pan, B. Yuan, Y. Li, D. He, *Chem. Commun.* **2010**, *46*, 2280 – 2282; d) H.-L. Jiang, T. Akita, T. Ishida, M. Haruta, Q. Xu, *J. Am. Chem. Soc.* **2011**, *133*, 1304 – 1306.

[7] a) D. Esken, X. Zhang, O. I. Lebedev, F. Schröder, R. A. Fischer, *J. Mater. Chem.* **2009**, *19*, 1314 – 1319; b) J. Hermannsdörfer, R. Kempe, *Chem. Eur. J.* **2011**, *17*, 8071 – 8077.

[8] a) Y. E. Cheon, M. P. Suh, *Angew. Chem.* **2009**, *121*, 2943 – 2947; *Angew. Chem. Int. Ed.* **2009**, *48*, 2899 – 2903; b) Y. E. Cheon, M. P. Suh, *Chem. Eur. J.* **2008**, *14*, 3961 – 3967; c) C. Zlotea, R. Campesi, F. Cuevas, E. Leroy, P. Dibandjo, C. Volkringer, T. Loiseau, G. Férey, M. Latroche, *J. Am. Chem. Soc.* **2010**, *132*, 2991 – 2997.

[9] M. Sabo, A. Henschel, H. Fröde, E. Klemm, S. Kaskel, *J. Mater. Chem.* **2007**, *17*, 3827 – 3832.

[10] T. Ishida, M. Nagaoka, T. Akita, M. Haruta, *Chem. Eur. J.* **2008**, *14*, 8456 – 8460.

[11] M. S. El-Shall, V. Abdelsayed, A. E. R. S. Khder, H. M. A. Hassan, H. M. El-Kaderi, T. E. Reich, *J. Mater. Chem.* **2009**, *19*, 7625 – 7631.

[12] Y. K. Hwang, D.-Y. Hong, J.-S. Chang, S. H. Jhung, Y.-K. Seo, J. Kim, A. Vimont, M. Daturi, C. Serre, G. Férey, *Angew. Chem.* **2008**, *120*, 4212 – 4216; *Angew. Chem. Int. Ed.* **2008**, *47*, 4144 – 4148.

[13] M. Müller, S. Hermes, K. Käher, M. W. E. van den Berg, M. Muhler, R. A. Fischer, *Chem. Mater.* **2008**, *20*, 4576 – 4587.

[14] a) P. J. Wesson, S. Soh, R. Klajn, K. J. M. Bishop, T. P. Gray, B. A. Grzybowski, *Adv. Mater.* **2009**, *21*, 1911 – 1915; b) Y. Wei, P. J. Wesson, I. Kourkine, B. A. Grzybowski, *Anal. Chem.* **2010**, *82*, 8780 – 8784; c) S. Soh, M. Byrska, K. Kandere-Grzybowska, B. A. Grzybowski, *Angew. Chem.* **2010**, *122*, 4264 – 4294; *Angew. Chem. Int. Ed.* **2010**, *49*, 4170 – 4198; d) Y. Wei, S. Soh, M. M. Apodaca, J. Kim, B. A. Grzybowski, *Small* **2010**, *6*, 857 – 863; e) B. A. Grzybowski, *Chemistry in Motion: Reaction-Diffusion Systems for Micro- and Nanotechnology*, Wiley, New York, **2009**, chap 4, pp. 61 – 91.

[15] a) Y. Yamada, C. K. Tsung, W. Huang, Z. Huo, S. E. Habas, T. Soejima, C. E. Aliaga, G. A. Somorjai, P. Yang, *Nat. Chem.* **2011**, *3*, 372 – 376.

[16] R. A. Smaldone, R. S. Forgan, H. Furukawa, J. J. Gassensmith, A. M. Z. Slawin, O. M. Yaghi, J. F. Stoddart, *Angew. Chem.* **2010**, *122*, 8812 – 8816; *Angew. Chem. Int. Ed.* **2010**, *49*, 8630 – 8634.

[17] Y. Wei, S. Han, D. Walker, S. Warren, B. A. Grzybowski, *Chem. Sci.* **2012**, *3*, 1090 – 1094.

[18] T. Huang, F. Meng, L. Qi, *J. Phys. Chem. C* **2009**, *113*, 13636 – 13642.

[19] Y. Wei, R. Klajn, A. O. Pinchuk, B. A. Grzybowski, *Small* **2008**, *4*, 1635 – 1639.